2014

Optimizing Sensor Layouts in Wave Farms

Jia Lu
Lehigh University

Optimizing Sensor Layouts in Wave Farms

By

Jia Lu

Presented to the Graduate and Research Committee

of Lehigh University

in Candidacy for the Degree of

Master of Science

in

Industrial and Systems Engineering

Lehigh University

April 2014

This thesis is accepted and approved in partial fulfillment of the requirement for the Master of Science.

_____

Date: April 2014

_____

Thesis Advisor: (Lawrence V. Snyder)

_____

Chairperson of Department: (Tamas Terlaky)

Acknowledgements

I want to thank my parents for constant supporting me in my study and life. I also want to thank Professor Larry Snyder, member of the Lehigh University wave energy group, for his patience, encouragement and guidance in my researching and modeling. In addition, I want to thank Professor Rick Blum, member of the Lehigh University wave energy group, Basel Alnajjab, the PhD candidate of Lehigh University and Yuhai Hu, the PhD candidate of Lehigh University for their help in my thesis.

Contents

List of Figures

List of Tables

Abstract

Wave energy and related devices have attracted more and more attention. The need for an accurate prediction system for ocean waveforms is urgent. Past research has involved the basic mathematical models and theories of predicting waveforms. The Cramer Rao Bound (CRB) is the key value to describe the accuracy of these models. The general form of the CRB has been derived in previous works, which also proposed several recommendations for the layout of sensors. However, the recommended layouts are not optimal, and the models do not capture the complicated ocean wave environment. In this thesis, three models which are used to find near-optimal solutions under different ocean wave environments are introduced. These models, which involve more factors of a realistic environment, are introduced and tested. Several better layouts under particular conditions are also presented. In addition, based on the computational results some recommendations for sensor layouts are given.

Chapter 1

Introduction

1.1 Wave Energy

As society develops, energy has become one of the most central issues. Our fast-developing economy and increasing needs from human beings all require more energy. Though the energy efficiency has been largely improved, the decreasing resources of traditional fossil fuels pushes humans to develop more renewable energy. In addition, the growing threat of global warming, which is a by-product of utilizing fossil fuels, makes the need for renewable energy even more urgent. Wave energy is one of the most promising forms of renewable energy.

Wave energy is the transport of energy by ocean surface waves and the conversion of that energy to do useful work like electricity generation so that the energy can be easily and conveniently transmitted and used. Among all forms of renewable energy, wave energy is a late starter. Unlike solar energy and wind energy, wave energy is now an immature form of energy and the related research is at the beginning. However, the potential of wave energy is

huge. Wave energy is more consistent and predictable than solar and wind energy, which is an important feature for electricity generation. There are already several experimental wave farms all over the world [1-5]. In the future, there is likely to be a place for wave energy in commercial electricity generation.

A wave energy converter (WEC) is a device used to convert wave energy to electricity. In general, there are five categories of WECs. They are known as Wave Activated Bodies, Oscillating Water Columns, Point Absorbers, Attenuators, and Overtopping Devices [3, 5, 6].

Wave Activated Bodies, as their name suggests, are devices with moving elements that are activated by the cyclic oscillation of the waves. Such devices directly transfer the kinetic energy of ocean waves into electric current. The DEXA is one illustrative example. DEXA is developed and patented by DEXA Wave Energy APS. A scaled prototype has been placed in the Danish part of the North Sea. This scaled prototype can generate 160 kW mean annual power [5, 7].

Oscillating Water Columns (OWCs) are a popular type of wave energy devices. Their function is similar to that of a wind turbine that is used for wind energy. OWCs can be placed both offshore and on the shoreline. An example of an offshore OWC is Sperboy developed by Embley Energy LTD. Its capacity is up to 450 kW mean annual power. A near-shore example is REWEC-3 created by the Università degli Studi "Mediterranea" di Reggio Calabria [8].

Point Absorbers are another popular type of device. They are buoy-type WECs that absorb wave energy from all directions. They are often placed offshore at or near the ocean surface. They function like an internal combustion engine. A vertical submerged floater harvests wave energy which is converted by a piston or similar device into electricity. One famous example is OPT's PowerBuoy Wave Generation System. Current projects of PowerBuoy have been operated in several places all over the world [9]. Another example is FO3 developed by Norwegian entrepreneur Fred Olsen. This device can produce up to 2.52 MW [10].

Attenuators are made of a series of floating sections. As waves pass, the sections will move up and down relative to each other. The energy of the moving sections will be captured in a common hydraulic line and converted into electric current. An example is Wave Star developed by Wave Star ApS [1].

Overtopping Devices work like a hydroelectric dam. They can be partitioned into near-shore and off shore. Wave Dragon is an example of an off shore device that is developed by Wave Dragon ApS and SeaWave Slot-Cone Generator (SSG) is a near shore devices. There is already much literature about the details of these devices [2]. For more information see Section 1.4.

1.2 Waveform Prediction

Like many other new scientific disciplines, most research in this area has first focused on the mechanism, hardware design, and control system of the WEC itself. Researchers have been more eager to improve the craft and efficiency of the WECs. However, as all these

physical factors mature, the cost of continuing to improve these factors is getting higher and higher. This situation has made many engineers transfer their sights to external factors. In addition, based on feedback from the companies at the forefront wave energy technology, they need a system capable of monitoring and predicting ocean waveforms to help them to control the WECs better. Therefore, waveform prediction has received much more attention in recent years.

A system to monitor waveforms at one location and point in time and predict waveforms at other locations and points in time can improve the efficiency of these devices and also make wave energy more useful for practical application. There are many studies about predicting the statistical description of waves [11, 12] but very few are related to predicting the exact waveform at a specific location and time in a noisy environment. In this thesis, prediction is achieved using a set of distributed sensors based on noisy measurements. Our research is concentrated on finding the optimal layout of sensors that can be used in a complicated ocean environment. Though our research is only for single frequency direction ocean environments, this is a good start for understanding more complicated environments. We base our analysis on the Cramer Rao Bound（CRB）and Fisher Information Matrix (FIM). More details can be found in the following sections.

1.3 Ocean Waves

Our objective is to improve the accuracy of the prediction of future waveforms by using multiple sensors. First, it is necessary to explain how to model ocean waves. For the analysis in this thesis, several assumptions are adopted. The first assumption is that the ocean is an

ideal incompressible fluid with no loss of mechanical energy. The assumption that fluid motion is irrotational and that the wave amplitudes are small enough to make linear theory applicable are also used. Moreover, the monitoring area in the ocean is deep enough that finite-depth effects such as dispersion are small. Finally, we assume that the waves were created by forcing functions, distant storms for example, that were applied at sufficient distances away resulting in the observation of fully developed ocean waves. With the assumptions described above, an ocean wave can be considered as a plane wave consisting of a sum of sinusoids with different directions, frequencies, amplitudes, wavelengths and phases [13-15].

Under this condition, [13] provides a general expression for the exact waveform seen at a particular location and time, in terms of several common characterizations of fluid flow (Surface Elevation, Vertical Surface Velocity, Vertical Surface Acceleration, etc.). If the particular point is located at a position $(x, y)^T$ on the surface of the ocean, then [13] show that the waveform at this point and time t is

$$\Phi(x,y,t) = \sum_{i=1}^{M}\sum_{j=1}^{L} A_{i,j} w_j^a \cos^b(\beta_i) sin^c(\beta_i) cos^d\big(|k_j| x\cos(\beta_i) + |k_j| y \sin(\beta_i) - t w_j + \phi_{i,j}\big) \sin^e\big(|k_j| x \cos(\beta_i)|k_j| + y \sin(\beta_i) - t w_j + \phi_{i,j}\big)\left(\frac{1}{g}\right)^f \quad (1)$$

In this expression, $A_{i,j}$ is the amplitude in meters, w_j is the frequency in radians per second, β_i is the angular direction in radians which is measured relative to the x axis, $\phi_{i,j}$ is the phase in radians, and k_j is the wave number. In addition, different value combinations of constant "a" through "f" denote different ocean wave characterizations. Table 1.1 [13] shows the particular value of each integer constant for different ocean wave characterizations.

Table 1.1: Integer Constant Values for Particular Ocean Flow Characterizations.

Sensor Measurement	a	b	c	d	e	f
Surface Elevation	0	0	0	1	0	0
Vertical Surface Velocity	1	0	0	0	1	0
Vertical Surface Acceleration	2	0	0	1	0	0
Displacement (x-axis)	0	1	0	0	1	0
Displacement (y-axis)	0	0	1	0	1	0
Velocity (x-axis)	1	1	0	1	0	0
Velocity (y-axis)	1	0	1	1	0	0
Acceleration (x-axis)	2	1	0	0	1	0
Acceleration (y-axis)	2	0	1	0	1	0
Surface Slope (x-axis)	2	1	0	0	1	1
Surface Slope (y-axis)	2	0	1	0	1	1

[13] argue that under the deep-water assumption made above, expression (1) can be simplified to

$$\Phi(x,y,t) = \sum_{i=1}^{M}\sum_{j=1}^{L} A_{i,j} w_j^a \cos^b(\beta_i)\sin^c(\beta_i)\cos^d\left(\left(\frac{w_j^2}{g}\right)x\cos(\beta_i) + \left(\frac{w_j^2}{g}\right)y\sin(\beta_i) - tw_j + \phi_{i,j}\right)\sin^e\left(\left(\frac{w_j^2}{g}\right)x\cos(\beta_i) + \left(\frac{w_j^2}{g}\right)y\sin(\beta_i) - tw_j + \phi_{i,j}\right)\left(\frac{1}{g}\right)^f \quad (2)$$

1.4 Literature Review

In the 1970s, wave energy started to capture the attention of scientists. Therefore, research in this area is still at the beginning. Today, most papers still concentrate on the mechanisms and control of the WEC systems. In [16], the authors discussed experimental and numerical results for the system's dynamics with simple and practical latching control techniques that do not require the prediction of waves or wave forces. Falcao [17] introduced a control method to maximize the output of a OWC system. Falnes [18] discussed a method to operate the OWC at full capacity in a rather large fraction of their lifetime with controlling the oscillation in order to approach an optimum interaction between the WEC and the incident wave. Both [17, 18] believed there are still advancements in improving the efficiency of the OWC system by optimizing the control system. Therefore, future work needs to focus more on the control part. From [16-18], we can understand that the current research of ocean wave energy focuses more on the control system but not on the prediction of waveforms. However, from these related works it is still clear that a key factor in the efficiency of WECs is how to make the WECs adapt to the complicated wave environment.

In the spirit of the tremendous work related to the control of WEC, there are also a group of scientists studying the idea of improving the performance of WEC devices by predicting future waveforms [11, 12, 19]. Li et al. [19] found that deterministic sea wave prediction combined with optimal constrained control can improve the efficiency of a WEC dramatically. However, most of them see the waveform prediction part as auxiliary to the control system and few papers focus on studying the performance of sensors themselves, especially sensor performance under noise. Esteva [11] and Panicker [12] both discussed using sensors to estimate the directional wave spectra. But neither of them attempted to

estimate the waveforms at an exact time. However, because there are few papers related to waveform prediction, these two papers provided us some valuable intuitions of this area.

The paper which is most related to this thesis is [13]. In this paper, the authors focused on sensor performance under a noisy environment. They derived an expression for the Cramer Rao Bound (CRB) from using a set of sensors for predicting short-term waveforms at a specific location in the wave farm. In addition, the authors also gave the CRB results from using different types of sensors under multiple wave conditions. Through a comparison, they discussed the optimal choices of sensor type for measuring and the optimal sensor layouts under a range of wave directions.

This thesis is aimed at identifying the optimal sensor layouts. However, the starting point is to think about this question from an optimization model perspective. We analyze the CRB of different combinations of sensor types under different layouts with different wave directions. It is impossible to find a single layout of sensors which is optimal under all conditions and it is also impractical to change the sensor layouts frequently due to different wave conditions. Therefore, in this thesis, we build stochastic and robust models to find the layouts which can produce a relatively low CRB for all wave conditions.

Chapter 2

General Model of Cramer Rao Bound for Wave Prediction

When doing estimation our goal is always to make an accurate estimate. However, prediction error always exists. How can we find a good unbiased estimator to represent our unknown parameter? The answer comes from the Cramer Rao Bound (CRB). The CRB is a lower bound on the minimum mean square prediction error that can be achieved by any unbiased estimator, an estimator that produces zero error on average.

In this chapter, a general expression for the CRB will be introduced. In addition, the important Fisher Information Matrix (FIM) will also be included. We also discussed the expressions for the CRB and FIM under a simple ocean wave condition. Furthermore, this chapter involved some particular characteristics of the CRB and FIM. The result of this chapter will be the foundation of the calculation of the CRB and analysis of prediction errors of all kinds of wave characterizations listed in Table 1.1.

2.1 General Models of Cramer Rao Bounds

The expression (2) which introduces a general sensor measurement is assumed as the basic measurement. The location of sensors are described by a position vector (x_r, y_r) in which r=1 … N. Therefore, the noisy sensor measurements at site r can be defined as:

$$\phi(t_m, x_r, y_r) = \Phi(t_m, x_r, y_r) + v_r(t_m), \qquad t_m = T_s, \dots, KT_s \tag{3}$$

In this expression, T_s is a sampling period and $v_r(t_m)$ is Gaussian white noise. Gaussian noise is a type of noise that has its probability density function equal to a normal distribution and white noise is a random signal with a constant power spectral density. Following [13], we collect the unknown parameters in (2) in a vector

$$\theta = \left(A_{1,1}, \dots, A_{M,L}, \beta_1, \dots, \beta_M, w_1, \dots, w_L, \phi_{1,1}, \dots, \phi_{M,L}\right)^T \tag{4}$$

From this expression, θ is a 2ML+M+L dimensional vector.

The Gaussian white noise term $v_r(t_m)$ is assumed to be a jointly Gaussian vector with mean 0, covariance $(\sigma_1^2, \dots, \sigma_{NK}^2)$ for sensor r=1,…,N and sampling period kT_s. The likelihood function of θ then will be

$$f_{\underline{\Phi}}(\underline{\Phi}, \theta) = \prod_{r=1}^{N} \prod_{k=1}^{K} \frac{1}{\sqrt{2\pi\sigma_{r,k}^2}} exp\left(-\frac{\left(\phi(kT_s, x_r, y_r) - \Phi(kT_s, x_r, y_r)\right)^2}{2\sigma_{r,k}^2}\right) \tag{5}$$

$\Phi(x_p, y_p, t_p)$ comes from (2) and it represents the value that needs to be predicted at a particular location (x_p, y_p) and a particular time t_p. Let $\widehat{\Phi}(x_p, y_p, t_p)$ be an unbiased estimator of $\Phi(x_p, y_p, t_p)$. Unbiased estimators must satisfy the equation below:

$$E_\theta = \{\widehat{\Phi}(x_p, y_p, t_p)\} = \Phi(x_p, y_p, t_p) \tag{6}$$

Based on the equation (6), the mean square error (MSE) of any unbiased estimation must will have the bound [20]:

$$MSE_{\widehat{\Phi}(x_p,y_p,t_p)} \geq qJ(\theta)^{-1}q^T = CRB_{\widehat{\Phi}(x_p,y_p,t_p)} \tag{7}$$

The value of the right side of this equation is our Cramer Rao Bound (CRB). Then, from the right-hand side of the inequality in (7), the elements of the CRB can be found. The CRB is described as the product of the row vector

$$q = \left(\frac{\partial\Phi(x_p,y_p,t_p)}{\partial\theta_1}, \dots, \frac{\partial\Phi(x_p,y_p,t_p)}{\partial\theta_{2ML+M+L}}\right) \tag{8}$$

and the Fisher Information Matrix (FIM) $J(\theta)$, which is a $(2\mathrm{ML} + \mathrm{M} + \mathrm{L}) \times (2\mathrm{ML} + \mathrm{M} + \mathrm{L})$ dimensional vector matrix whose element (l, n) is calculated as [13, 20, 21]

$$J_{l,n}(\theta) = E\left\{\frac{\partial}{\partial\theta_l}\ln f_{\underline{\Phi}}(\underline{\Phi};\theta)\frac{\partial}{\partial\theta_n}\ln f_{\underline{\Phi}}(\underline{\Phi};\theta)\right\} \tag{9}$$

The research in this thesis is about prediction under Gaussian white noise, in which case equation (9) can be simplified to:

$$J_{l,n}(\theta) = \sum_{r=1}^{N}\sum_{k=1}^{K}\frac{1}{\sigma_{r,k}^2}\left(\frac{\partial}{\partial\theta_l}\Phi(x_r, y_r, kT_s)\right)\left(\frac{\partial}{\partial\theta_n}\Phi(x_r, y_r, kT_s)\right) \tag{10}$$

From (10), the calculation of each entry of the FIM will include two derivatives. The number of entries in *J* will be huge if the number of plane waves M and each frequency component L are huge because this case will result in a large number of unknown parameters. If we only consider the simplest case in which the wave environment monitored only consists of one single wave (M=L=1), the vector of wave parameters (4) is

$$\theta = \left(A_{1,1}, \beta_1, w_1, \phi_{1,1}\right)^T \tag{11}$$

and the Fisher Information Matrix has the simple form

$$J(\theta) = \begin{pmatrix} J_{1,1} & J_{1,2} & J_{1,3} & J_{1,4} \\ J_{2,1} & J_{2,2} & J_{2,3} & J_{2,4} \\ J_{3,1} & J_{3,2} & J_{3,3} & J_{3,4} \\ J_{4,1} & J_{4,2} & J_{4,3} & J_{4,4} \end{pmatrix} \tag{12}$$

Since each entry of the FIM consists of two derivatives there is a need to know the derivative form of any ocean wave characterization in (2). [13] have derived each derivative form. Therefore, we will only use them instead of deriving them again.

2.2 Cramer Rao Bounds under a Single Wave Condition

This thesis aims to give some intuition into the behavior of sensors. Therefore, it focuses on some simple wave conditions. We use derivative forms in [13] to derive the simplest wave

condition in which the ocean wave is assumed to be a single wave (M=L=1). In this section we also assume that the noise at each sensor can be considered as independent and identically distributed. This assumption ensures that $\sigma_1 = \sigma_2 = \cdots = \sigma_{NK}$ so that the calculation will be simplified. The monitored area is also restricted to lie in a finite area. This makes sure that the sensors cannot be placed at an infinite distance from the farm. In addition, we assume that every sensor will be used to estimate the same types of wave characterizations. The combinations of sensors that estimate different types will not be included in this thesis.

A given sensor can only estimate a limited number of types of characterizations each time. In this thesis, the case in which a sensor is used to estimate only three types of characterizations is considered. Actually, the estimation model of each type is almost the same but only differs by the values of a through f in Table 1.1. Therefore, in this section, we will only introduce one model.

2.2.1 Model of q under Single Wave Condition

From expression (7), the CRB is the product of q and the FIM. Hence, first the expression of q needs to be derived for this simplest wave ocean environment. Since M=L=1, q will be

$$q = \left(\frac{\partial \Phi(x_p, y_p, t_p)}{\partial A_{1,1}}, \frac{\partial \Phi(x_p, y_p, t_p)}{\partial \beta_1}, \frac{\partial \Phi(x_p, y_p, t_p)}{\partial w_1}, \frac{\partial \Phi(x_p, y_p, t_p)}{\partial \phi_{1,1}} \right) \tag{13}$$

For each element of q, the expressions will be

$$\frac{\partial}{\partial A_{1,1}}\Phi(x_p, y_p, t_p) = w_1^a \cos\left(\left(\frac{w_1^2}{g}\right)x_p\cos(\beta_1) + \left(\frac{w_1^2}{g}\right)y_p\sin(\beta_1) - t_p w_1 + \phi_{1,1}\right) \tag{14}$$

$$\frac{\partial}{\partial \beta_1}\Phi(x_p, y_p, t_p) = -A_{1,1}w_1^a \sin\left(\left(\frac{w_1^2}{g}\right)x_p\cos(\beta_1) + \left(\frac{w_1^2}{g}\right)y_p\sin(\beta_1) - t_p w_1 + \phi_{1,1}\right) \quad \left(\left(\frac{w_1^2}{g}\right)y_p\cos(\beta_1) - \left(\frac{w_1^2}{g}\right)x_p\sin(\beta_1)\right) \tag{15}$$

$$\begin{aligned}\frac{\partial}{\partial w_1}\Phi(x_p, y_p, t_p) = \\ = -A_{1,1}w_1^a \sin\left(\left(\frac{w_1^2}{g}\right)x_p\cos(\beta_1) + \left(\frac{w_1^2}{g}\right)y_p\sin(\beta_1) - t_p w_1\right. \\ \left. + \phi_{1,1}\right)\left(\left(\frac{2w_1}{g}\right)x_p\cos(\beta_1) + \left(\frac{2w_1}{g}\right)y_p\sin(\beta_1) - t\right) \\ + aA_{1,1}w_1^{a-1}\cos\left(\left(\frac{w_1^2}{g}\right)x_p\cos(\beta_1) + \left(\frac{w_1^2}{g}\right)y_p\sin(\beta_1) - t_p w_1 + \phi_{1,1}\right)\end{aligned} \tag{16}$$

$$\frac{\partial}{\partial \phi_{1,1}}\Phi(x_p, y_p, t_p) = -A_{1,1}w_1^a \sin\left(\left(\frac{w_1^2}{g}\right)x_p\cos(\beta_1) + \left(\frac{w_1^2}{g}\right)y_p\sin(\beta_1) - t_p w_1 + \phi_{1,1}\right) \tag{17}$$

This is the expression of each element in q. Notice that in expression (13)-(17) the location (x_p, y_p) and time t_p are the particular location and time we want to estimate. They are different from the locations of sensors (x_r, y_r) and time sampling period $\mathrm{k}T_s$.

2.2.2 Model of FIM under Single Wave Condition

In this section an exploit for each element in the Fisher Information Matrix (FIM) is given. First starting from the diagonal entries of the FIM. The $J_{1,1}$ term is

$$J_{1,1}(\theta) = \frac{1}{\sigma^2}\sum_{r=1}^{N}\sum_{k=1}^{K}\left(\frac{\partial}{\partial A_{1,1}}\Phi(x_r, y_r, kT_s)\right)\left(\frac{\partial}{\partial A_{1,1}}\Phi(x_r, y_r, kT_s)\right)$$

$$= \frac{w_1^{2a}}{\sigma^2}\sum_{r=1}^{N}\sum_{k=1}^{K}\frac{1}{2}\left(1+\cos(2\psi - 2w_1 kT_s)\right) \tag{18}$$

In this expression,

$$\psi = \left(\frac{w_1^2}{g}\right)x_r\cos(\beta_1) + \left(\frac{w_1^2}{g}\right)y_r\sin(\beta_1) + \phi_{1,1} \tag{19}$$

ψ represents the time-independent part of the argument of the cosine function.

The $J_{2,2}$ term is

$$J_{2,2}(\theta) = \frac{1}{\sigma^2}\sum_{r=1}^{N}\sum_{k=1}^{K}\left(\frac{\partial}{\partial \beta_1}\Phi(x_r, y_r, kT_s)\right)\left(\frac{\partial}{\partial \beta_1}\Phi(x_r, y_r, kT_s)\right)$$

$$= \frac{A_{1,1}^2 w_1^{4+2a}}{g^2\sigma^2}\sum_{r=1}^{N}\left((x_r, y_r)\cdot U_{\beta_1}\right)^2\sum_{k=1}^{K}\frac{1}{2}\left(1+\cos(2\psi - 2w_1 kT_s)\right) \tag{20}$$

$U_{\beta_1} = \left(-\sin(\beta_1), \cos(\beta_1)\right)$ is the unit vector perpendicular to the wave direction β_1.

The $J_{3,3}$ term is

$$J_{3,3}(\theta) = \frac{1}{\sigma^2}\sum_{r=1}^{N}\sum_{k=1}^{K}\left(\frac{\partial}{\partial w_1}\Phi(x_r, y_r, kT_s)\right)\left(\frac{\partial}{\partial w_1}\Phi(x_r, y_r, kT_s)\right)$$

$$= \frac{1}{\sigma^2}\sum_{r=1}^{N}\sum_{k=1}^{K}\left(-A_{1,1}w_1^a \sin(\psi - kT_s w_1)\left(\frac{2w_1}{g}(x_r, y_r)\cdot V_{\beta_1} - kT_s\right)\right.$$
$$\left. + aA_{1,1}w_1^{a-1}\left(\cos(\psi - w_1 kT_s)\right)\right)^2 \tag{21}$$

$V_{\beta_1} = \left(\cos(\beta_1), \sin(\beta_1)\right)$ is the unit vector parallel to the wave direction β_1.

The $J_{4,4}$ term is

$$J_{4,4}(\theta) = \frac{1}{\sigma^2}\sum_{r=1}^{N}\sum_{k=1}^{K}\left(\frac{\partial}{\partial \phi_{1,1}}\Phi(x_r, y_r, kT_s)\right)\left(\frac{\partial}{\partial \phi_{1,1}}\Phi(x_r, y_r, kT_s)\right)$$

$$= \frac{A_{1,1}^2 w_1^{2a}}{\sigma^2}\sum_{r=1}^{N}\sum_{k=1}^{K}\frac{1}{2}\left(1 - \cos(2\psi - 2w_1 kT_s)\right) \tag{22}$$

Next, we consider the off-diagonal entries.

$$J_{1,2}(\theta) = \frac{1}{\sigma^2}\sum_{r=1}^{N}\sum_{k=1}^{K}\left(\frac{\partial}{\partial A_{1,1}}\Phi(x_r, y_r, kT_s)\right)\left(\frac{\partial}{\partial \beta_{1,1}}\Phi(x_r, y_r, kT_s)\right)$$

$$= \frac{-A_{1,1}w_1^{2+2a}}{g\sigma^2}\sum_{r=1}^{N}\left((x_r, y_r)\cdot U_{\beta_1}\right)\sum_{k=1}^{K}\cos(\psi - w_1 kT_s)\sin(\psi - w_1 kT_s) \tag{23}$$

$$J_{1,3}(\theta) = \frac{1}{\sigma^2}\sum_{r=1}^{N}\sum_{k=1}^{K}\left(\frac{\partial}{\partial A_{1,1}}\Phi(x_r, y_r, kT_s)\right)\left(\frac{\partial}{\partial w_1}\Phi(x_r, y_r, kT_s)\right)$$

$$= \frac{-1}{\sigma^2}\sum_{r=1}^{N}\sum_{k=1}^{K}\Bigg(A_{1,1}w_1^a\sin(\psi - kT_s w_1)\left(\frac{2w_1}{g}(x_r, y_r)\cdot V_{\beta_1} - kT_s\right) + aA_{1,1}w_1^{a-1}\left(\cos(\psi - w_1 kT_s)\right)\Bigg)\left(w_1^a\cos(\psi - kT_s w_1)\right) \tag{24}$$

$$J_{1,4}(\theta) = \frac{1}{\sigma^2}\sum_{r=1}^{N}\sum_{k=1}^{K}\left(\frac{\partial}{\partial A_{1,1}}\Phi(x_r, y_r, kT_s)\right)\left(\frac{\partial}{\partial \phi_{1,1}}\Phi(x_r, y_r, kT_s)\right)$$

$$= \frac{-A_{1,1}w_1^{2a}}{\sigma^2}\sum_{r=1}^{N}\sum_{k=1}^{K}\cos(\psi - w_1 kT_s)\sin(\psi - w_1 kT_s) \tag{25}$$

$$J_{2,3}(\theta) = \frac{1}{\sigma^2}\sum_{r=1}^{N}\sum_{k=1}^{K}\left(\frac{\partial}{\partial w_1}\Phi(x_r, y_r, kT_s)\right)\left(\frac{\partial}{\partial \beta_1}\Phi(x_r, y_r, kT_s)\right)$$

$$\approx \frac{1}{\sigma^2}\sum_{r=1}^{N}\sum_{k=1}^{K} A_{1,1}^2 w_1^{2a}\sin^2(\psi - w_1 kT_s)\left(\frac{2w_1}{g}\left((x_r, y_r)\cdot V_{\beta_1}\right) - kT_s\right)$$

$$\left(\frac{w_1^2}{g}\left((x_r, y_r)\cdot U_{\beta_1}\right)\right) \tag{26}$$

$$J_{2,4}(\theta) = \frac{1}{\sigma^2}\sum_{r=1}^{N}\sum_{k=1}^{K}\left(\frac{\partial}{\partial\beta_1}\Phi(x_r, y_r, kT_s)\right)\left(\frac{\partial}{\partial\phi_{1,1}}\Phi(x_r, y_r, kT_s)\right)$$

$$= \frac{A_{1,1}^2 w_1^{2+2a}}{g\sigma^2}\sum_{r=1}^{N}\left((x_r, y_r)\cdot U_{\beta_1}\right)\sum_{k=1}^{K}\sin^2(\psi - w_1 kT_s) \tag{27}$$

$$J_{3,4}(\theta) = \frac{1}{\sigma^2}\sum_{r=1}^{N}\sum_{k=1}^{K}\left(\frac{\partial}{\partial w_1}\Phi(x_r, y_r, kT_s)\right)\left(\frac{\partial}{\partial\phi_{1,1}}\Phi(x_r, y_r, kT_s)\right)$$

$$= \left(-A_{1,1}w_1^a\sin(\psi - kT_s w_1)\left(\frac{2w_1}{g}(x_r, y_r)\cdot V_{\beta_1} - kT_s\right)\right.$$
$$\left. + aA_{1,1}w_1^{a-1}\cos(\psi - w_1 kT_s)\right)\left(-A_{1,1}w_1^a\sin(\psi - w_1 kT_s)\right) \tag{28}$$

In [13], Alnajjab and Blum also give an approximation for each term. With this kind of approximation the features of each term corresponding to the location of a sensor can be found. However, in this thesis the major task is finding the optimal locations of sensors, so

the features of each term in the Fisher Information Matrix are not considered. These features can be found from the final optimization directly.

The final Fisher Information Matrix is given by

$$\mathrm{J}(\theta) = \begin{pmatrix} J_{1,1} & J_{1,2} & J_{1,3} & J_{1,4} \\ J_{1,2} & J_{2,2} & J_{2,3} & J_{2,4} \\ J_{1,3} & J_{2,3} & J_{3,3} & J_{3,4} \\ J_{1,4} & J_{2,4} & J_{3,4} & J_{4,4} \end{pmatrix} \tag{29}$$

the reason the term $J_{1,2}$ is equal to $J_{2,1}$ is that both $J_{1,2}$ and $J_{2,1}$ are the products of $\frac{\partial \Phi(x_p, y_p, t_p)}{\partial A_{1,1}}$ and $\frac{\partial \Phi(x_p, y_p, t_p)}{\partial \beta_1}$. The only difference is the sequence. However, since these two derivatives are independent of each other the sequence can be changed. Therefore, this two terms are exactly the same and the other pair of terms are also the same.

2.2.3 Singularities of Fisher Information Matrix

According to [13], the FIM will be singular under some conditions. This means that the estimators will have very poor performance. Therefore, when using this theory to calculate the CRB such conditions should be avoided. This section introduces several conditions that will result in a singular FIM and the method to avoid this problem when modeling.

The most obvious case happens when a non-vertical sensor (either measuring x-axis or y-axis characterizations) are used to measure the features under the condition that the wave direction is perpendicular to the features it measured; for example, using a sensor to measure the velocity along X axis. If the wave comes from right along the Y axis the result of the

measurement will be zero. Another condition which will generate a singular FIM is when the number of collected measurements is not sufficient. If the number of measurements is less than the number of unknown parameters in expression (4) the FIM will be singular. Furthermore, in [13] Alnajjab and Blum also gave a more complicated case that will result in a singular FIM. However, this condition is beyond the scope of this thesis so we will not talk about it here.

To solve the problem mentioned above, in this thesis different methods are used. For the first condition, when modeling this problem the wave directions 0, $\frac{\pi}{2}$ and π are avoided. The models in this thesis assume we are using 8 sensors to estimate 4 unknown parameters. The number of measurements is larger than the number of unknown parameters so the second condition and third condition are also avoided.

Chapter 3

Optimization Models

In this chapter, three different optimization models for locations of sensors will be proposed. In [13], Alnajjab and Blum gave some suggested locations of sensors in several particular conditions and the trend of CRB versus changes in the characterizations of the ocean waves. However, there are some limitations in [13]. First, in [13] Alnajjab and Blum only considered sensor that can measure one type of characterization at a time. In reality, sensors can measure multiple types of characterization at the same time. Therefore, one major task of this thesis is to consider such a condition. When measuring different types of characterizations, the optimal location of the sensors will be different for each type of characterization. Our objective is to find an optimal layout of these sensors to provide good performance for different characterizations simultaneously. Second, the optimal layout given by [13] is derived from the features of some diagonal entries in the FIM. In this thesis, we will use our optimization models to justify the suggested layout from [13] so that the result is much more convincing. Third, in the model from [13], ocean waves come from all directions with equal probability. However, the real condition is much more complicated, with waves more likely to come from some than from others. In this thesis, a stochastic

model will be built so that the complicated ocean wave environment can be modeled more accurately. Forth, in [13], the authors did not discuss how the CRB changes as the layout changes. In this thesis, the trend of the variance of the CRB corresponding to varying layouts will also be derived from the models. Furthermore, considering different types of characterizations the models in this thesis also give each type of characterizations a weight. With such a weight, the importance of each type of characterization can be indicated and based on the different importance the optimal layout of sensors will vary.

3.1 Notation

The following is the notation that will be used in the models.

- r = the index sensor r
- x_r = the x axis position of sensor r
- y_r = the y axis position of sensor r
- kT_s = the sampling period
- x_p = the x axis position of the point at which the waveform is to be estimated
- y_p = the y axis position of the point at which the waveform is to be estimated
- t_p = the time point at which the waveform is to be estimated

- β = the wave direction, relative to x axis, in radians

- $|B|$ = the total number of given wave direction

- i = the measured type of characterization (e.g if the sensor can measure every characterizations in Table 1.1, then I takes values 1,…,11)

- N = the total number of values of i

- ω_i = the weight of the i characterizations

- $f_\beta(\beta)$ = the probability of each wave direction

Among this notation, the location of the sensors (x_r, y_r) are the decision variables. The other pieces of notation are the parameters of the model.

3.2 General Model

The general model assumes the wave comes from each direction with equal probability. The objective function of this model is like

$$\min \sum_{i=1}^{N} \frac{1}{N} \sum_{\beta} \frac{1}{|B|} CRB_{(x_p, y_p, t_p)}\big((x_r, y_r), kT_s, i, \beta\big) \tag{30}$$

If each wave direction is assigned a weight ω_i, then the objective function becomes

$$\min \sum_{i=1}^{N} \omega_i \sum_{\beta} \frac{1}{|\mathrm{B}|} CRB_{(x_p,y_p,t_p)}\big((x_r, y_r), kT_s, i, \beta\big) \tag{31}$$

In this model, the particular location and time point at which the waveform must be estimated will be given. The time sampling period and possible wave directions will also be given. The weights ω_i need to be decided. If one of the selected characterizations is much more important than others the weight of this one should be much higher than that of the others. This model will find the optimal layout of sensors that makes the weighted average CRB of the selected types of characterizations smallest under multiple wave directions.

For example, consider a setting in which the wave direction ranges from 0.1 rad to 0.5 rad (in increments of 0.1). The location and time point we want to measure are (0, 0) and 100 s. The sampling period is the first 100 s. The elevation, displacement (x axis) and displacement (y axis) are the desired characterizations, with equal weights. Then the model will be as follows

$$\min \sum_{i=1}^{3} \frac{1}{3} \sum_{\beta=0.1}^{0.5} \frac{1}{5} CRB_{(0,0,100)}\big((x_r, y_r), 100, i, \beta\big) \tag{32}$$

3.3 Stochastic Model

In the stochastic model, the probability of each wave direction will be considered. The model is given by

$$\min \sum_{i=1}^{N} \omega_i \sum_{\beta} f_\beta(\beta) CRB_{(x_p, y_p, t_p)}\big((x_r, y_r), kT_s, i, \beta\big) \tag{33}$$

The difference between the general model and this stochastic model is the term $f_\beta(\beta)$. This term is the probability of each wave direction. Since real ocean wave directions change over time, the stochastic model is much more realistic than the general one.

3.4 Robust Model

For the robust model, the objective aims to find the locations of sensors to minimize the maximum (i.e worst-case) CRB taken over all β. In this model, we are assuming the waves are equal likely to come from all directions in the given range. For a single characterization the model will be

$$\min max_\beta \left\{ CRB_{\left(x_p, y_p, t_p\right)} \left(\left(x_r, y_r\right), kT_s, i, \beta \right) \right\} \tag{34}$$

In this expression, wave direction can be any β in the given range B.

This robust model can also be used when multiple characterizations are desired. The difference is that this time the model finds the locations of sensors to minimize the maximum weighted average CRB, with the maximum taken over all β and the weighted average taken over all i. The expression will change to

$$\min max_{\beta} \left\{ \sum_{i=1}^{N} \omega_i \, CRB_{\left(x_p, y_p, t_p\right)} \left(\left(x_r, y_r\right), kT_s, i, \beta \right) \right\} \tag{35}$$

3.5 Solution Strategies

The basic strategies for these three models is a heuristic method. There are several reasons for why such a method is used. First, from expression (7) we can see the CRB is nonlinear. The CRB depends on q and the FIM. Both of them are related to decision variables, i.e., the sensor locations, via complicated nonlinear functions. Second, in a wave farm, there are typically more than 4 sensors. Adding one sensor location into the model will result in a geometric growth in the size of calculation. Therefore, considering too many sensors is hard. Third, the research on wave energy is at the beginning, and the features of measurements corresponding to complicated ocean wave environments are still not clear. Therefore, we cannot use intuition about the structure of the problem in order to reduce the search space.

Because of the difficulties above, in this thesis, we consider two sensors as a pair. This reduces the number of decision variables. In addition, we only consider moving one pair of sensors in the wave farm under several particular conditions. We use an enumeration method to find the optimal solution under these particular conditions.

Chapter 4

Computational Analysis

For a given number of sensors, different layouts will result in different values of the CRB. In addition, different layouts will optimize different objective functions. In this chapter, we will discuss changing locations of one pair of sensors in different layouts under different ocean wave conditions. Since adding more degrees of freedom will make the calculation difficulty increase tremendously, the results for moving more pairs are not considered in this thesis.

For our numerical results, we make several basic assumptions. The ocean environment in all the results below assumes $A_{1,1} = 2$ m, $\omega_1 = 1.6$ rad/s and $\phi_{1,1} = 1$ rad. We assume samples are collected for 8 seconds with a sampling frequency of 100 Hz. The CRB is calculated for the origin 100s ahead. The wave direction β is varies from 0.2 rad to 2.7 rad (about 10 degrees to 160 degrees). The location of the measured point is (0, 0). Most of the examples will have 8 sensors in need of illustrating more complicated condition. The other assumptions will be introduced separately for each model. We assume we wish to evaluate the CRB for surface elevation, displacement (x axis) and displacement (y axis).

We discretize the search place to optimize the sensor locations. We use a step size of 50 in our discretization. This number ensures the trend in the CRB is evident as the locations vary and also makes the calculation faster than a smaller step size. Figure 4.1 is an example of the distribution of the CRB with different discretization intervals (20, 30 and 50) under the same condition. The general trend of the CRB with different discretization intervals is almost the same. Hence, 50 is a reasonable value for this numerical analysis.

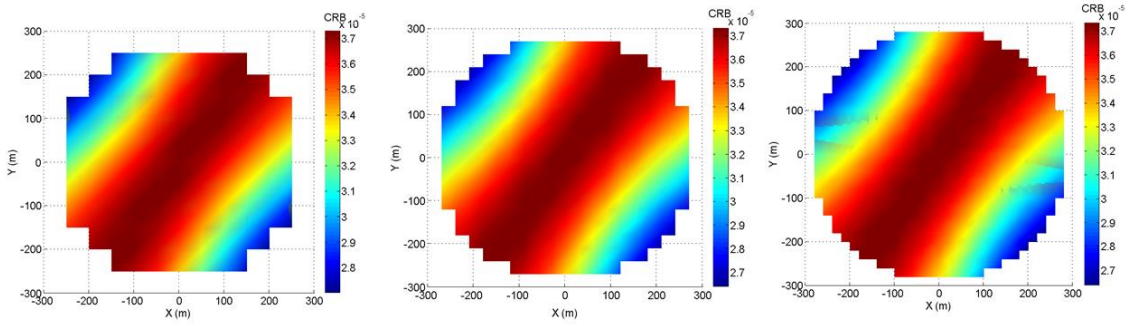

(a) (b) (c)

Figure 4.1(a) – (c): Comparison of Different Discretization Intervals (20, 30, 50)

4.1 General Model

For the general model, we first discuss the even layout introduced in [13] and use the general model to confirm the recommendation. In addition, some different results and improvements will also be discussed in this section.

4.1.1 Even Layout

In this layout, the 4 pairs of sensors are equally spaced on the perimeter of a circle of radius equal to 300 m. This layout depicted in Figure 4.2. Then, we try to move one pair of them both on the perimeter of the circle and in the interior of the circle. Since the sensors are equally spaced on the perimeter at the beginning there will be 4 choices of sensor pairs to move: The pair on the x axis (2, 4), the pair on the y axis (1, 3), the pair in quadrant 2 and 4 (5, 7) and the pair in quadrants 1 and 3 (6, 8).

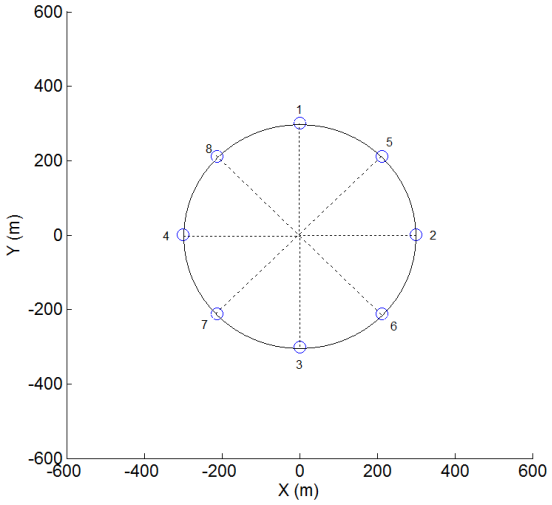

Figure 4.2: The Original Even Layout

When moving the pair of sensors (2, 4), since they are in one pair their coordinates will be (-x, -y) and (x, y). Figure 4.3 shows the change of CRB according to locations of this pair of sensors. Figure 4.3 indicates that as we move the pair towards the center of the farm the average value of the CRB will increase dramatically. The optimal location of this pair lies at (-300, 0) and (300, 0) (The reason why we cannot see these two points is because only the points (300, 0) and (-300, 0) are calculated around their areas. Therefore, there are only one

point here because our discretization interval is 50). The figure has a symmetric with respect to the y axis.

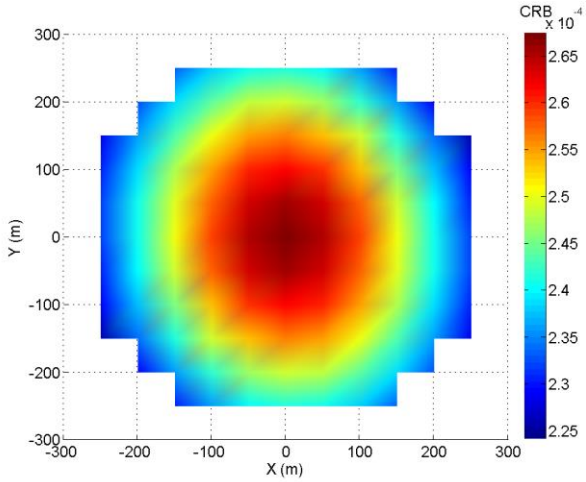

Figure 4.3: CRB as Function of Locations of Sensors (2, 4)

Figure 4.4 shows the CRB as the pair (1, 3) moves. This time, the line of symmetry is the x axis. The optimal locations are at (0, 300) and (0, -300). These locations are perpendicular to those for (2, 4).

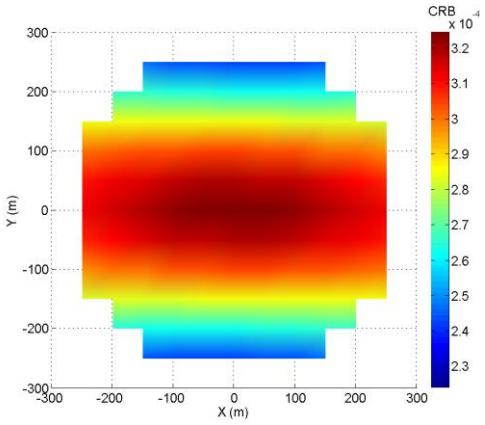

Figure 4.4: CRB as Function of Locations of Sensors (1, 3)

Figure 4.5 shows the CRB as the pair (5, 7) moves. The CRB is still symmetric with respect to an axis but the angle is totally different from the two conditions before. The optimal locations are at (-150, -250) and (150, 250).

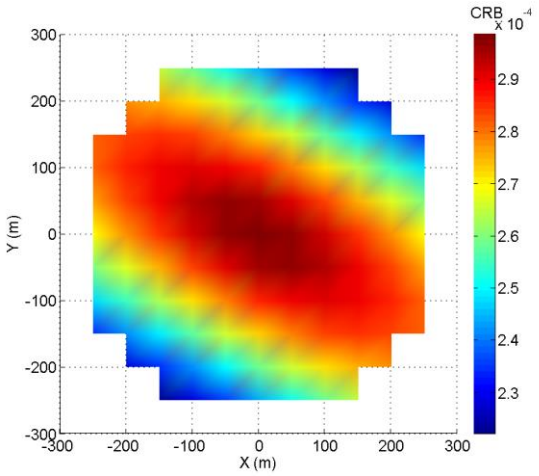

Figure 4.5: CRB as Function of Locations of Sensors (5, 7)

Figure 4.6 shows the CRB as the pair (6, 8) moves. The optimal locations are (-150,250) and (150, -250). This is exactly symmetric to Figure 4.5 along the y axis.

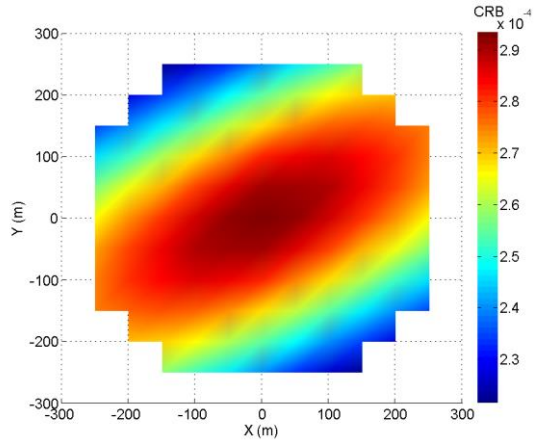

Figure 4.6: CRB as Function of Locations of Sensors (6, 8)

Comparing Figures 4.3 through 4.6 it is evident that the optimal locations of this pair of sensors have some characteristics. Each figure has an axis of symmetry and when locating the pair of sensors perpendicular to this axis as far as possible we will get the optimal solution. Actually, all of the figures suggest that the original even layout is the optimal layout. The reason why Figure 4.5 and Figure 4.6 give a slightly different location from the original one is that the discretization interval is 50 and many points cannot be evaluated. The reason why the optimal location is equally spaced on the perimeter of the circle is because of the range of wave direction and the weight of each characterizations. At the beginning of this chapter, the range of wave direction was assumed to be from 0 to π. Notice the wave direction β is relative to the x axis and in the general model the wave is assumed to come from 0 to π with equal probability. Therefore, the wave is evenly coming from all directions. Furthermore, in the general model, each measured CRB is equally weighted. Under such a condition, the suggested layout turns out to be even also.

This result also partially confirms the suggestion in [13]. The authors suggested that when the wave is equally likely to come from any direction (0 to π rad) the sensors should be placed with $\frac{\pi}{4}$ rad separation on the perimeter of a circle that has the maximum radius allowed. We say "partially" because in this thesis only one pair of sensors is changing and the other 3 pairs are fixed to be placed with $\frac{\pi}{4}$ rad separation. Because of relatively low calculation speed more complicated situations are not considered in this thesis. However, the model in this thesis would give the optimal solution if enough time were allowed for computation.

In addition, under this condition, if we change the weights of the 3 characterizations or change the range of wave direction, the optimal layout will also change. Assume that the displacement (x axis) is more important than other two characterizations. The three weights are

$$\omega_1 = 0.7;\ \omega_2 = 0.15;\ \omega_3 = 0.15. \tag{36}$$

The original location of the changed sensors is (300, 0) and (-300, 0). The distribution of CRB is as given in Figure 4.7.

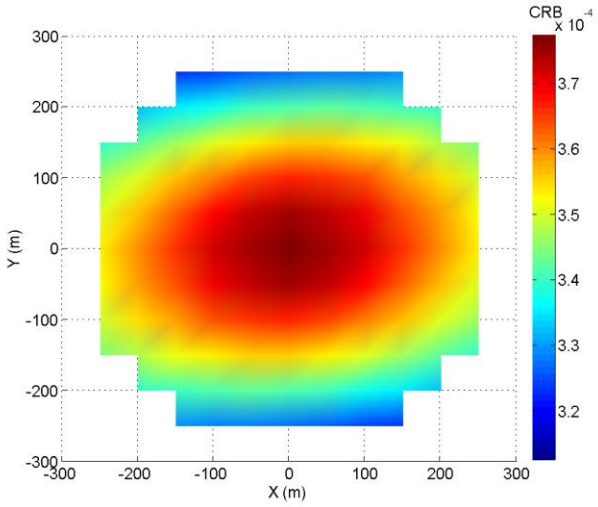

Figure 4.7: Distribution of CRB under Unequal Weights of 3 Characterizations

From Figure 4.7 the optimal location of sensors is no longer the original location. Continuing to put this pair of sensors at their original location will yield a relatively bad result. Instead, the optimal solution is at a location near the y axis. When the displacement (x axis) is a more important characterization the axis of symmetry will be the x axis, which results in the optimal location at a position that is perpendicular to it as far as possible. From the result

of this model the optimal solution is at (0, 300) and (0, -300), which is exactly the farthest location perpendicular to the axis of symmetry. If one change the weights to other combinations, the optimal layout will again change.

If the range of wave directions changes what would be the result? Assume the three characterizations are equally weighted. This time, the range of wave directions is from 0.2 rad to 1.47 rad. The CRB is given in Figure 4.8.

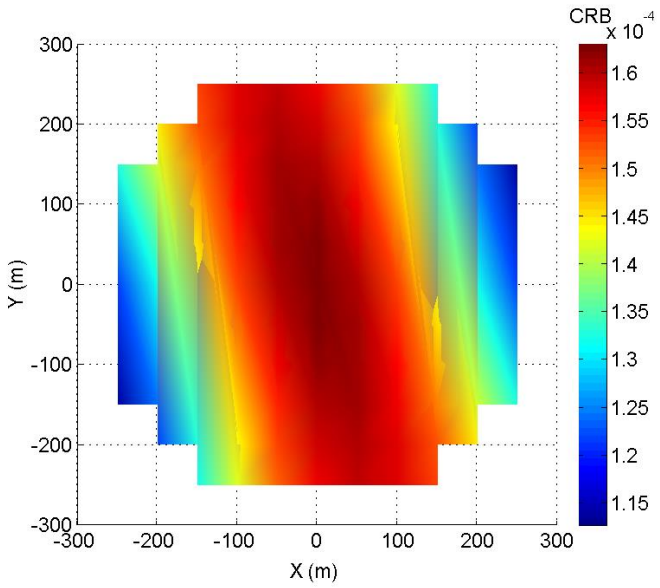

Figure 4.8: Distribution of CRB when Wave Direction Ranges from 0.2 rad to 1.47 rad

This time the axis of symmetry is to the y axis, rotated slightly counterclockwise and the optimal solution also changes with the axis of symmetry. Therefore, the analysis above suggests that the significant part of deciding the locations of the sensors is to find where the axis of symmetry is, or what the factors are that influence the axis of symmetry.

4.1.2 Improved Solution for General Model

Our approach for the general model can also find some better layouts than those suggested in [13]. In [13], the authors gave the recommendation that for equally likely wave directions, the sensors should be placed perpendicular to the endpoints of the range and as far as possible from each other. For example, [13] suggested that when the ocean wave is equally likely to come from any angle in interval $\left[\frac{3}{8}\pi, \frac{5}{8}\pi\right]$ the layout should be the one depicted in Figure 4.9.

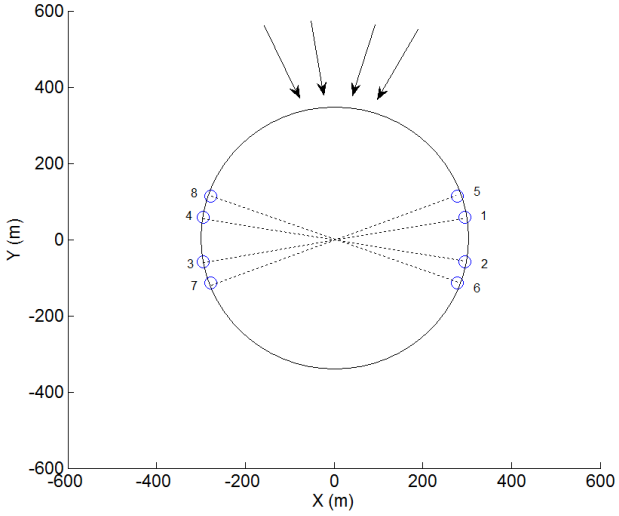

Figure 4.9: Original Layout From [13]

However, using our general model, a better layout has been found. Figure 4.10 shows the layout suggested by our general model.

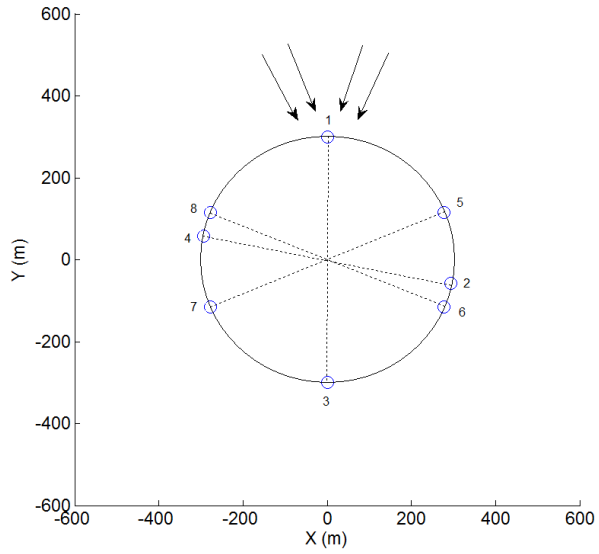

Figure 4.10: New Layout Recommended by General Model

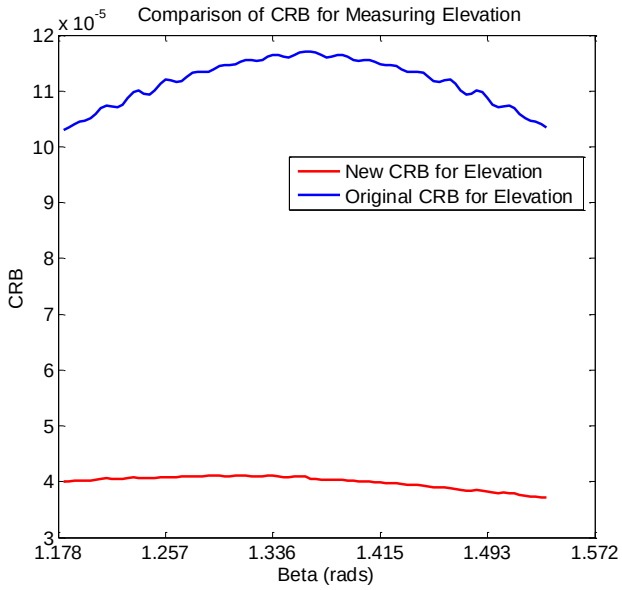

(a)

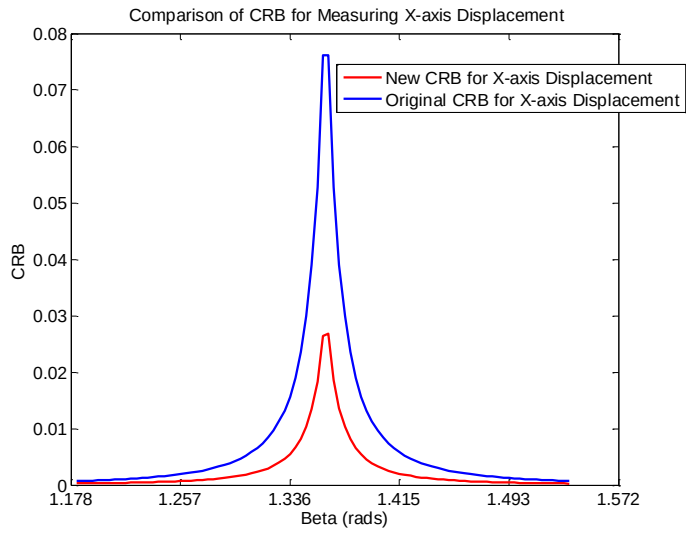

(b)

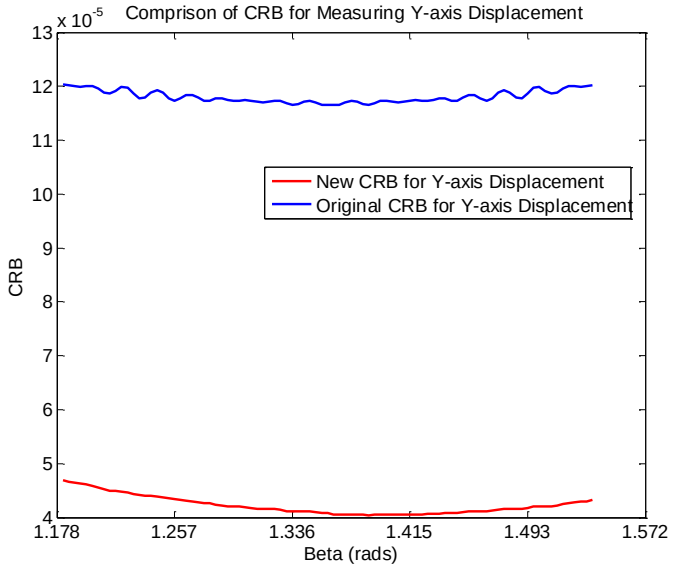

(c)

Figure 4.11 (a) - (c): Comparisons between Original Layout and Optimized General Model Layout

Figure 4.11 gives the CRB as a function of wave direction β, for both the original and new layouts for the three wave characterizations (Surface Elevation, Displacement (x axis),

Displacement (y axis)). In Figure 4.11 (b) the peak occurs because the wave direction is near the y axis and the objective is displacement (x axis) so we have a very poor performance at the middle as mentioned in Chapter 3.

From these three comparisons it is clear that the new layout will produce a better result. All of the three CRB have been reduced. Certainly, this layout may not be the optimal one since only the locations of one pair have been changed. However, this suggested that the conclusion in [13] is inaccurate. The performance is not always good if sensors are located following the recommendation. When the wave direction is in the range from 0 to π with equal probability and the weight of each characterization are equal, then the layout that is evenly placed on the allowed maximum radius will always give a good performance. However, when the range is reduced to $\frac{\pi}{4}$ the conclusion seems to lose its accuracy. In [13], they got their conclusion from studying each entry of the Fisher Information Matrix, but from this thesis it seems there are other factors that will influence the final result. The relation between the wave direction and the layout is not that simple. Furthermore, since in this thesis only one pair of sensors is moved there might be even better layout if more pairs are moved, but because of the low calculation speed this was not attempted in this thesis.

4.2 Stochastic Model

For more complicated ocean wave environments the waves will come from different directions with unequal probability. Stochastic models are appropriate for such a condition. The wave direction has a significant effect on the layout of sensors. The following example will show the different levels of performance under the same ocean wave environment.

Three characterizations are desired: surface elevation, displacement (x axis) and displacement (y axis). Their weights are set to be equal. The wave come from the range $[0.2, 2.7]$ rad. In Section 4.1 with the general model we find that the even layout has a relatively good performance under this condition. Now, different probabilities are given to each direction. Will the even layout still be a good one? Figure 4.12 gives the result. We still only move one pair of sensors (2, 4) and fix other three pairs. The wave direction is 0.2 rad, 0.7rad, 1.2 rad, 1.7 rad, 2.2 rad and 2.7 rad. The probabilities of each direction are 0.1, 0.1, 0.1, 0.3, 0.3 and 0.1, respectively. This time the even layout is no longer the best one.

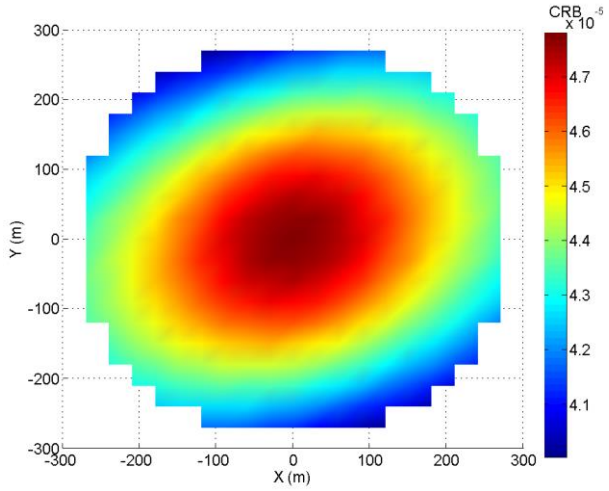

Figure 4.12: Value of Average CRB under Uneuqal Probability Wave Direction

Figure 4.12 suggests the optimal locations should be around (120, -270) and (-120, 270). The resolving layout is shown in Figure 4.13.

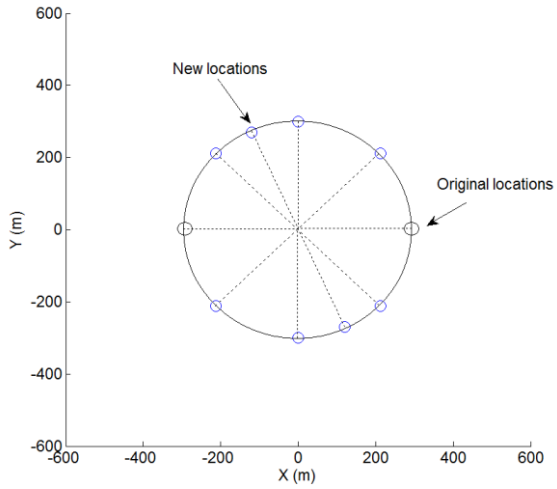

Figure 4.13: New Layout Recommended by Stochastic Model

Table 4.1: Comparison of CRB between Even Layout and Recommended New Layout Found by Stochastic Model.

	x_1	y_1	x_2	y_2	Average CRB of All Directions	CRB of Elevation	CRB of Displacement (x axis)	CRB of Displacement (y axis)
Even Layout	300	0	-300	0	0.000042978	0.000031654	0.000215356	0.000037268
New Layout	120	270	-120	270	0.000040037	0.000024859	0.000259335	0.000027455

Table 4.1 shows each CRB for the two layouts. Except the CRB of displacement (x axis), all CRBs are better for the new layout. Therefore, the stochastic model can find a more suitable layout by considering the probability of wave direction. This stochastic model is more practical since the real ocean wave environment is full of uncertainty. In some areas of the ocean, the wave environment is different from other areas. The waves in this area will come from some particular directions with higher probabilities. The stochastic model in this thesis is a good way to find the optimal layout in such an ocean wave environment.

4.3 Robust Model

Because of the definition of the robust model, it is more useful when the CRB of the desired characterization changes heavily with a change in the wave direction. In this section, an example is given in which displacement (x axis) is measured. The CRB of the displacement (x axis) changes heavily with a change in the wave direction [13]. The wave direction in this example is in the range from 0.2 rad to 1.2 rad. Only one pair of sensors (2, 4) is moved and the other three pairs remain fixed. The original layout is the even layout introduced in Section 4.1. After running the robust model, the best location of this pair should be around (180, 240) and (-180, 240). Figure 4.14 shows a comparison of the CRB of displacement (x axis) under the two different layouts.

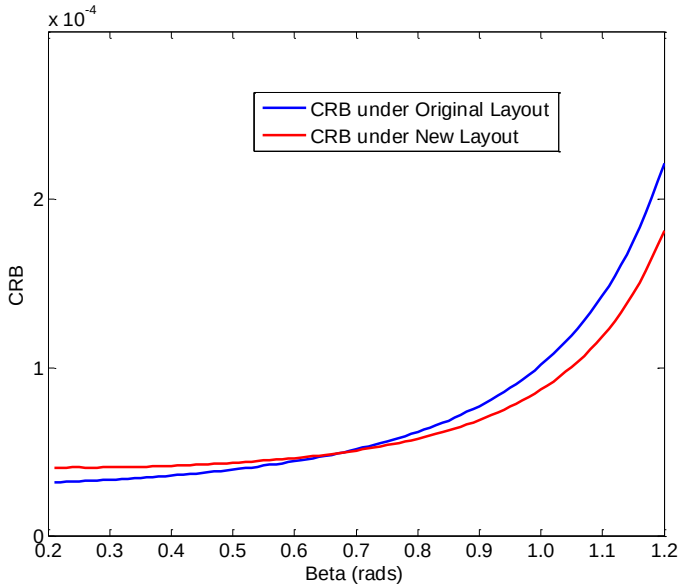

Figure 4.14: Comparion between Original Layout and Robust Model Layout

From Figure 4.14, though from 0.2 rad to 0.7 rad the original layout has better performance, the new layout recommended by the robust model has a better performance

for $\beta > 0.7$ rad. Such a layout makes the measurement system much more stable and at the same time maintains good performance of the measurement system. Therefore, when the desired characterization varies heavily under different ocean wave environments, using the robust model can help to find a layout with relatively stable performance.

Chapter 5

Conclusion

In the first chapter of this thesis, we discussed the general issues of renewable energy and ocean wave energy. The basic mechanics and devices are also introduced. Chapter 2 provides an overview of the key theories including the Cramer Rao Bound (CRB) and Fisher Information Matrix (FIM). In Chapter 3, we build three optimization models for finding the optimal layout of sensors: general model, stochastic model and robust model. They consider the optimal layout of sensors from three different angles. The general model is used to handle simple ocean wave environments assuming the wave are equal likely to come from different directions. The stochastic model adopts the assumption that different wave directions have different probabilities. The robust model finds a layout which can optimize the worst-case performance. In Chapter 4, we present the computational analysis. In this chapter, the optimal solutions from the three models are shown. Given the limitation on run time, only one pair of sensors is moved. The even layout of sensors turns out to be a relatively good one under equal probability of wave direction. The recommended layout for equal probability of wave direction in [13] is also tested and modified. The stochastic model is used to find the optimal layout under unequal wave direction probability. A comparison between

the even layout and the layout found by the stochastic model is presented. The robust model is also involved in this part and the performance of the even layout and the layout recommended by the robust model are compared.

In the future, there is still a lot of work to be done and extended. The solution method for the models in this thesis is actually an enumeration method. Much more efficient algorithms should be developed so that the run time of the models can be reduced significantly. This thesis only considers moving one pair of sensors, with the other pairs of sensors fixed. Therefore, the solutions in this thesis certainly may not be optimal because there are many other combinations which have not been evaluated. The models include several realistic factors like the probability of wave direction and the weight of each characterization. However, this is far from a complete description of the real ocean environment. More realistic factors should be included in the models. In addition, this thesis presents models that are used to find the optimal layout but offers no information why these layouts are optimal. Therefore, it is also worth investigating the true relations between the layout of sensors and the ocean wave environment. Furthermore, future research should also focus on the behavior of sensors under irregular (multi-component) ocean waves.

Bibliography

[1] L. Marquis, M. Kramer, and P. Frigaard, "Performance Evaluation of the Wavestar Prototype," in *EWTEC 2011 conference in Southampton, UK*, 2011, pp. 06-09.

[2] L. Margheritini, D. Vicinanza, and P. Frigaard, "SSG wave energy converter: Design, reliability and hydraulic performance of an innovative overtopping device," *Renewable Energy,* vol. 34, pp. 1371-1380, 2009.

[3] Shalinee Kishore, Lawrence Snyder, and P. Pradhan, "Ocean Wave Energy: Technologies, Opportunities and Challenges," *IEEE Smart Grid Newsletter,* 2013.

[4] J. P. Kofoed and P. Frigaard, "Hydraulic evaluation of the LEANCON wave energy converter," Department of Civil Engineering, Aalborg University, Aalborg. DCE Technical Reports, 2008.

[5] J. Kofoed, "Hydraulic evaluation of the DEXA wave energy converter," Department of Civil Engineering, Aalborg University, Aalborg. DCE Technical Reports, 2009.

[6] J. McGrath. *How Wave Energy Works*. Available: HowStuffWorks.com.

[7] L. Martinelli, B. Zanuttigh, and J. P. Kofoed, "Statistical analysis of power production from OWC type wave energy converters," *Proc. EWTEC,* 2009.

[8] P. Boccotti, "On a new wave energy absorber," *Ocean Engineering,* vol. 30, pp. 1191-1200, 2003.

[9] K. Edwards, J. E. Eder, P. R. Hart, and D. A. Montagna, "Development of Wave Energy Converters at Ocean Power Technologies," 2011.

[10] A. Leirbukt and P. Tubaas, "A wave of renewable energy," *ABB Review,* vol. 3, pp. 29-31, 2006.

[11] D. Esteva, "Wave direction computations with three gage arrays," *Coastal Engineering Proceedings,* vol. 1, pp. 349-362, 1976.

[12] N. Panicker and L. E. Borgman, "Directional spectra from wave-gage arrays," *Coastal Engineering Proceedings,* vol. 1, pp. 117-133, 1970.

[13] B. Alnajjab and R. S. Blum, "Ocean wave prediction from noisy sensor measurements " in *Proceedings of the 1st Marine Energy Technology Symposium*, Washinton, D.C., 2013.

[14] J. Falnes, *Ocean Waves and Oscillating Systems*: Cambridge University Press, 2002.

[15] G. B. Whitham, *Linear and Nonlinear Waves*: John Wiley & Sons, 2011.

[16] M. Lopes, J. Hals, R. Gomes, T. Moan, L. Gato, and A. d. O. Falcao, "Experimental and numerical investigation of non-predictive phase-control strategies for a point-absorbing wave energy converter," *Ocean Engineering,* vol. 36, pp. 386-402, 2009.

[17] A. d. O. Falcão, "Control of an oscillating-water-column wave power plant for maximum energy production," *Applied Ocean Research,* vol. 24, pp. 73-82, 2002.

[18] J. Falnes, "Optimum control of oscillation of wave-energy converters," *International Journal of Offshore and Polar Engineering,* vol. 12, pp. 147-154, 2002.

[19] G. Li, G. Weiss, M. Mueller, S. Townley, and M. R. Belmont, "Wave energy converter control by wave prediction and dynamic programming," *Renewable Energy,* vol. 48, pp. 392-403, 2012.

[20] S. M. Kay, *Fundamentals of Statistical Signal Processing, Volume I: Estimation Theory (v. 1)*: Prentice Hall, 1993.

[21] H. L. Van Trees, *Detection, Estimation, and Modulation Theory, Optimum Array Processing*: John Wiley & Sons, 2004.

[22] L. Christensen, E. Friis-Madsen, and J. P. Kofoed, "The Wave Energy Challenge: the Wave Dragon case," in *POWER-Gen Europe*, 2005.

[23] L. J. Mao, "Optimizing Wave Farm Layouts Under Uncertainty," Master's Thesis, Lehigh University, 2013.

[24] P. K. Mehta, "Reducing the environmental impact of concrete," *Concrete International,* vol. 23, pp. 61-66, 2001.

[25] J. Paul and I. Davies, "Effects of copper-and tin-based anti-fouling compounds on the growth of scallops (Pecten maximus) and oysters (Crassostrea gigas)," *Aquaculture,* vol. 54, pp. 191-203, 1986.

Vita

The author was born in China in 1989. He was awarded bachelor degree with honor in Thermal Energy and Power Engineering in Dalian University of Technology in 2012. Following that, he spent two years in studying Industrial & System Engineering in Lehigh University. During that, he jointed Lehigh University wave energy group to investigate optimization of sensor layouts in wave farms. By 2014, he finished his M.S. project in Lehigh University.